Hierarchy in the halogen activation during surface-promoted Ullmann coupling

Néstor Merino-Díez,[a, b, c] Alejandro Pérez Paz,[d] Jingcheng Li,[b] Manuel Vilas-Varela,[e] James Lawrence,[a, c] Mohammed S. G. Mohammed,[a, c] Alejandro Berdonces-Layunta,[a, c] Ana Barragán,[c, f] J. Ignacio Pascual,[b, g] Jorge Lobo-Checa,[h] Diego Peña,[e] and Dimas G. de Oteyza*[a, c, g]

Abstract: Within the collection of surface-supported reactions currently accessible for the production of extended molecular nanostructures under ultra-high vacuum, Ullmann coupling has been the most successful in the controlled formation of covalent single C-C bonds. Particularly advanced control of this synthetic tool has been obtained by means of hierarchical reactivity, commonly achieved by the use of different halogen atoms that consequently display distinct activation temperatures. Here we report on the site-selective reactivity of certain carbon-halogen bonds. We use precursor molecules halogenated with bromine atoms at two non-equivalent carbon atoms and found that the Ullmann coupling occurs on Au(111) with a remarkable predilection for one of the positions. Experimental evidence is provided by means of scanning tunneling microscopy and a rationalized understanding of the observed preference is obtained from density functional theory calculations.

Introduction

A continuous boost of computing power is at the core of current technology roadmaps. So far, the most promising approach in this pursuit involves the maximization of the number of electronic components per integrated circuit. With silicon-based technology reaching scaled-down saturation, single molecules displaying basic electronic functionalities (rectifiers, switches…) are among the most promising alternatives for the substitution of current electronic components[1]. However, an effective manufacturing of molecular electronics requires a precise control of the structure not only within the functional elements but also of their respective linkage. In this context, on-surface synthesis represents a promising platform for the implementation of molecular electronics[2]. Besides expanding the synthetic routes available for creating different forefront materials, it results in designed materials that readily feature suitable two-dimensional structure for their subsequent implementation into planar integrated circuits[3].

Aiming at their successful integration in future devices, such functional materials require mechanical robustness and high electron mobility, for which covalent bonds stand out when compared to weaker interactions[4]. Inspired by conventional wet-chemistry, numerous reactions yielding C-C bond formation have already been achieved on surfaces, including Sonogashira coupling[5], aldehyde-amine coupling[6] or Glaser coupling[7] among others[8]. Nevertheless amid this collection of C-C generating reactions, Ullmann coupling (UC), in which two aryl halides are coupled on a catalytic surface (such as the facets of commonly used coinage metals) to form a biaryl molecule, represents the most widespread one to date[9]. A milestone in the development of UC as the leading on-surface synthesis reaction scheme was set by Grill and coworkers[10], who demonstrated how the morphology and dimensionality of molecular networks can be precisely tuned by adding halogen atoms at different linking sites within the same precursor backbone. Ever since, UC has been tested on a large number of different substrates and aromatic precursors[11], highlighting its versatility for the on-surface formation of different low-dimensional nanostructures.

Advanced control of on-surface synthesis protocols has been obtained through hierarchical processes[12]. That is, controlled sequences of reactions which promote the correct step-by-step connection of molecules in the formation of complex molecular structures. With UC, this hierarchy can be achieved by functionalizing the carbon backbone with different halogens, since each of them features different energy barriers for the scission of its carbon-halogen bond[13]. In this work we show how, even when using the same halogens, a selective activation of specific C-Br bonds can be obtained by different means, namely depending on their location within the same aromatic precursor. Our combined scanning tunneling microscopy (STM) and density functional theory (DFT) simulations results reveal that

[a] N. Merino-Díez, Dr. J. Lawrence, M. S. G. Mohammed, A. Berdonces-Layunta, Dr. Dimas G. de Oteyza
Donostia International Physics Center (DIPC)
20018 San Sebastián, Spain
E-mail: d_g_oteyza@ehu.eus
[b] N. Merino-Díez, Dr. J. Li, Dr. J. I. Pascual
CIC nanoGUNE, nanoscience cooperative research center
20018 San Sebastián, Spain
[c] N. Merino-Díez, Dr. J. Lawrence, M. S. G. Mohammed, A. Berdonces-Layunta, A. Barragán, Dr. Dimas G. de Oteyza
Centro de Física de Materiales – MPC, CISC-UPV/EHU
20018 San Sebastián, Spain
[d] Dr. A. Pérez Paz
School of Physical Sciences and Nanotechnology, Yachay Tech University
100119 Urcuqui, Ecuador
[e] M. Vilas-Varela, Dr. D. Peña
CIQUS, Centro Singular de Investigación en Química Biolóxica e Materiais Moleculares
15705 Santiago de Compostela, Spain
[f] A. Barragán
Departamento de Física de Materiales, Universidad del País Vasco (UPV/EHU)
20018 San Sebastián, Spain
[g] Dr. J. I. Pascual, Dr. D. G. de Oteyza
Ikerbasque, Basque Foundation for Science
48013 Bilbao, Spain
[h] Dr. Jorge Lobo-Checa
Instituto de Ciencia de Materiales de Aragón, CSIC-Universidad de Zaragoza 50009 Zaragoza

Supporting information for this article is given via a link at the end of the document.

this site-selectivity is driven by the substrate and the X shape conformation of the precursor. At the preferred adsorption configuration of the precursor, the halogens display different distances to the metal surface, which leads to a strongly modulated catalytic effect of the substrate for each C-Br bond.

Results and Discussion

In this experiment we make use of 2,2',10,10'-tetrabromo-9,9'-bianthracene (TBBA, Fig. 1a, see supporting information for the synthesis of this molecule). The reactivity of similar di-brominated bianthracene (DBBA) precursors, having halogen atoms located either at 10 and 10´ or at 2 and 2´ positions, has been previously reported for different coinage metal surfaces[14]. When bromine atoms are located at positions 2 and 2', UC governs the synthetic process and renders, after subsequent thermal cyclodehydrogenation (CDH), chiral graphene nanoribbons (chGNRs) on Au(111), Ag(111) and Cu(111) (Fig. 1c)[14]. Similarly, when bromine atoms are located at positions 10 and 10', armchair GNRs are obtained on Au(111) and Ag(111)[14] (Fig. 1b) through UC and CDH. However, the coupling selectivity given by the halogen excision is overruled by the substrate´s catalytic effect on Cu(111). In this case, new radicals are created via dehydrogenation at C_2 positions, which ultimately determine the polymerization motif and yield chGNRs upon CDH[14]. The fact that the same results are obtained even with non-halogenated bianthryl precursors demonstrate that this coupling mechanism is fully independent of whether radicals are present at 10,10´ positions or not[15]. These findings highlight the complex competition in the determination of the reaction mechanism between the halogen position within the aromatic skeleton and the specific interactions with the substrate. Here, we employ TBBA precursors (Fig. 1a) on Au(111) in an attempt to specifically address this interplay.

After TBBA deposition, UC is thermally-induced at ~450 K and TBBA precursors form bianthrylene polymers. Figure 2 shows different scale STM images of this phase. As observed also with either type of DBBA reactants, the polymers appear aggregated into islands, indicating the presence of attractive intermolecular forces. These polymers are seen as a series of zigzagging lobes corresponding to the up-pointing termini of anthracene subunits. The latter arrange in an alternatingly tilted non-planar configuration to minimize the steric hindrance exerted by the neighbouring hydrogen atoms. Because this zigzag-display is shared by both armchair and chiral GNRs[14], an unambiguous determination of the polymer structure is not straightforward at this point.

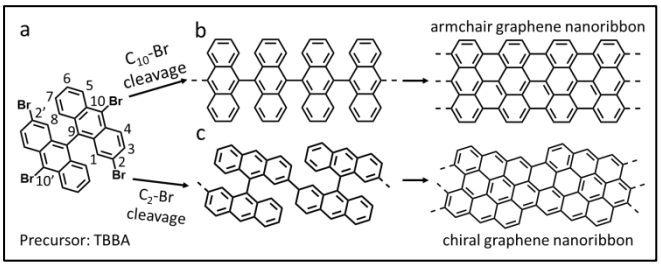

Figure 1. Possible synthetic routes expected in this experiment from (a) TBBA precursor. (b) C_{10}-Br cleavage leading to armchair GNRs formation (c) C_2-Br cleavage leading to chiral GNRs formation. Note that primed position x' is chemically equivalent to the corresponding unprimed position x and either would yield the same GNR.

Figure 2 also reveals the presence of a disordered network surrounding the polymeric islands and spreading over the remaining Au(111) surface. A closer look reveals that this web consists of single circular adsorbates arranged either in line or in a zigzag manner (Fig. S1). Similar networks have been observed for submonolayer coverages of halogens on Au(111)[16], as well as with other GNR precursors with a large stoichiometric halogen ratio,[17] which leads us to the conclusion that these adsorbates are bromine atoms. This kind of networks has not been observed in polymers formed from similar di-brominated precursors because the halogens are preferentially placed underneath the up-pointing anthracene ends, "hidden" from the scanning probe[18]. The observed Br network is thus assigned to the additional Br atoms as we change from dibrominated to tetrabrominated reactants, which can no longer be incorporated below the polymers. This finding underlines that both 2,2´ as well as 10,10´ positions are dehalogenated at this stage.

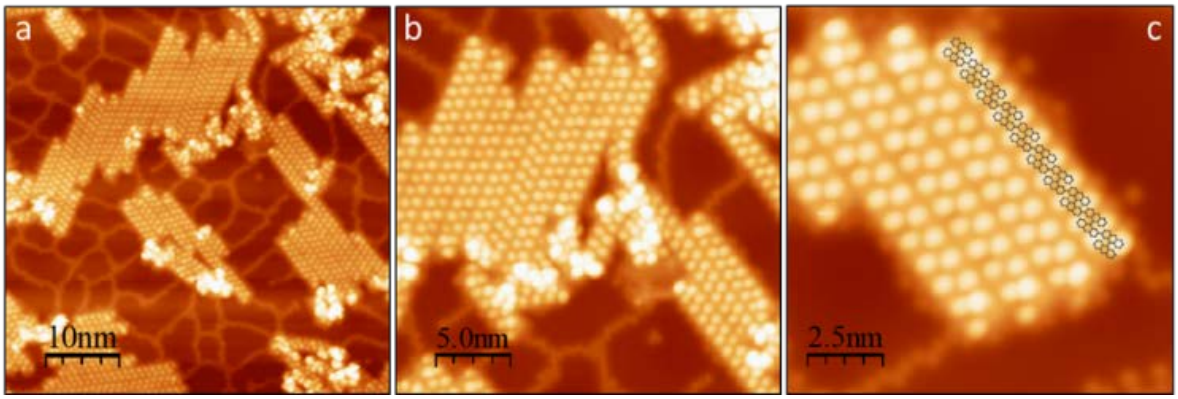

Figure 2. STM images of polymeric phase. (a) 50 nm² (U = 1.4 V, I = 140 pA). (b) 25 nm² (U = 1.4 V, I = 140 pA). (c) 12.5 nm² (U = 1.5 V, I = 1.0 nA) with superimposed wireframe model where only the carbon skeleton is shown.

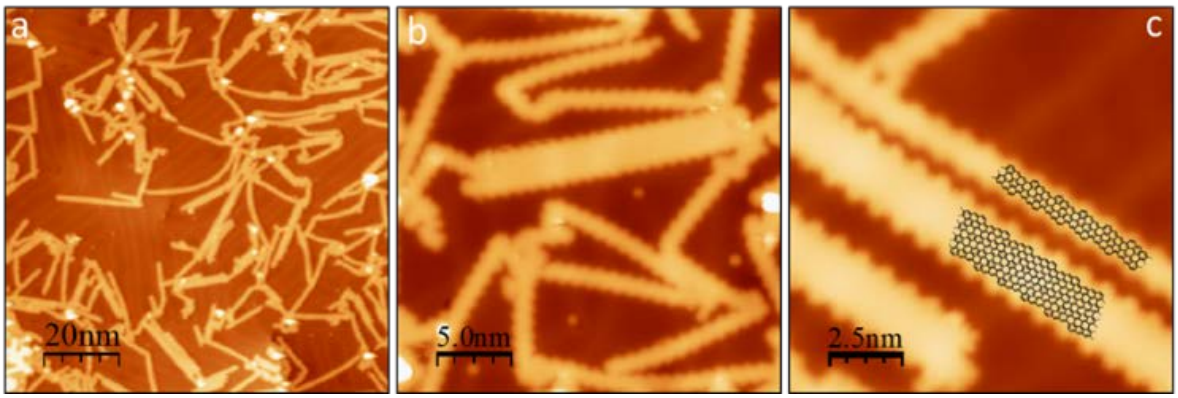

Figure 3. GNRs resulting from TBBA precursor. (a) 100 nm² (U = 1.1 V, I = 80 pA). (b) 25 nm² (U = 1.0 V, I = 120 pA). (c) 12.5 nm² (U = 50 mV, I = 0.5 nA) with superimposed wireframe models showing only the carbon backbone.

After polymerization, intramolecular CDH is induced by annealing the sample to higher temperatures, thereby turning the polymers into planar GNRs. At this point it is easy to identify from the lateral edge morphology that the resulting product is exclusively (3,1)-chGNRs (Fig. 3). This implies a dramatically favored UC via the 2,2' positions between the debrominated precursors, which given the well-known preferred reactivity of acenes at their central ring positions[19] is a surprising result. The UC itself being a multistep reaction, the observed preference may arise from any of the different steps. Reactant diffusion can be discarded because it would affect both halogen positions alike. A difference in the barriers associated to the bond formation between two nearby carbon radicals is also unlikely, since they are typically much lower than the barriers associated with the homolytic cleavage of the C-Br bonds[20]. Thus, the homolytic cleavage seems to be the determinign step.

We have indeed proved the sequential Br activation by temperature-dependent XPS measurements. Fig. 4 depicts the evolution of Br 3d core level spectra in the temperature range displaying the changes. At low temperatures, the spectra evidence two different sets of Br 3d doublets (marked with light and dark red arrows, respectively), each associated with one of the different Br pairs. As the temperature is risen, the doublet at higher binding energies dissappears first, with a relatively sharp transition temperature around 250 ºC. We thus associate this Br 3d doublet to the Br at 2,2´ positions. Subsequently, also the second doublet fades, although with a smoother temperature dependence. Concomitant with the dissappearance of those two core level doublets, a new one appears at more than 2 eV lower binding energies, associated with the atomic Br adsorbed on the metal surface. Its intensity profile as a function of temperature (at the energy marked with a dashed blue line), reveals two distinct increases that correlate with the activation temperatures of each of the 'organic Br pairs', marked respectively with light and dark red horizontal lines as a quide to the eye. Finally, at around 340 ºC the Br 3d core level intensity dissappears, evidencing the Br desorption from the surface. Because Br desorbs preferentially as HBr,[21] this desorption temperature can be associated with the cyclodehydrogenation temperature, at which H becomes available for Br atoms to combine with and desorb. Although the threshold temperature values extracted from the XPS and STM analyses differ, this may relate to the different chambers and temperature mesurement methods (pyrometer vs. thermocouple, respectively). However, most importantly their combination unambiguously reveals a stepwise activation of the different Br species within the reactant.

Figure 4. Photoemission spectra of the Br 3d core levels of precursor TBBA and their evolution as a function of sample annealing. At the right, an intensity profile at the energy marked with the dashed line reveals the two distinct intensity increases.

For a better understanding of the experimental findings we performed DFT calculations on this system. We studied the homolytic cleavage of C-Br bonds in TBBA and dibromoanthracene (DBA) molecules in the gas phase and found that the 10,10´ positions exhibit a slightly higher reactivity (i.e., a lower C-Br dissociation binding energy) than the 2,2´

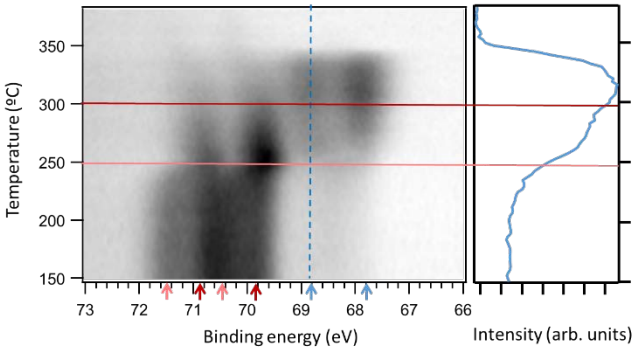

positions with a marginal difference of 1.1 kcal/mol for both molecules, suggesting that having an additional neighboring DBA subunit (as in TBBA) has a negligible impact on the dissociation binding energy of C-Br bonds (i.e., DBA and the more sterically congested TBBA have almost identical C-Br dissociation binding energies). The preference for 2,2´ positions for TBBA on Au(111) surface must thus have a different origin.

To address a possible influence of the substrate, we investigate the relative stability of two adsorption configurations in which the

C_2-Br can be either oriented towards (Fig. 5a) or away from (Fig. 5b) the surface. Both configurations show a dihedral angle between the anthracene subunits of ~127°, consistent with the relatively low energy cost (~5 kcal/mol) needed to distort from the 90° optimum angle calculated for TBBA molecule in gas phase (Fig. S3). We find that the adsorption geometry with C_2-Br pointing towards the surface is 0.387 eV more favorable, making it the dominant configuration on Au(111). Although as deposited molecules are difficult to image experimentally and display notable polymorphism and disorder, the best recognizable structure indeed fits an assembly of molecules with the C_2-Br pointing down (Fig. S4). Interestingly, in this conformation bromine atoms located at positions 2 and 2‘ are closer to the surface by ~0.27 Å than those at positions 10 and 10‘ (Fig. S5). A difference that may be further enhanced as the temperature increases, taking into account the vibrational modes of the respective C-Br bonds (with the C_2-Br bonds pointing towards the surface more than C_{10}-Br). As the homolytic cleavage of the C-Br bonds can be catalyzed by metallic substrates[20], we associate this proximity to the substrate with an enhanced catalytic effect on the C_2-Br bonds, which in turn promotes the polymerization along the 2,2´ rather than along the 10,10´ positions.

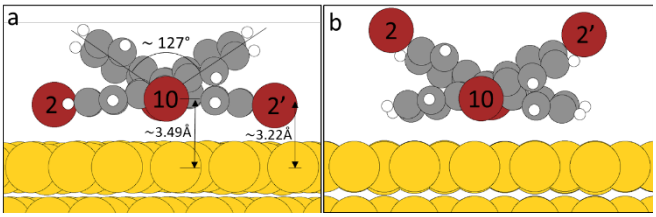

Figure 5. Simulated models for the adsorption of TBBA precursor on Au(111). Adsorption configuration with C_2-Br pointing (a) towards or (b) away from the surface. The yellow, gray, red, and white spheres represent the Au, C, Br, and H atoms, respectively.

Lastly, it is important to note that the chiral ribbons display a variety of widths, which in turn indicates a lateral fusion of the polymers. Although the cyclodehydrogenative fusion of GNRs has been reported earlier and would lead to similar results [22], in this particular case it can be discarded. The reason for this is that while samples prepared from 2,2´-DBBA reveal no lateral fusion of the chiral ribbons after annealing to temperatures of 590 K (Fig. S2), starting from TBBA at a similar coverage we observe wider, fused GNRs readily at 530 K (Fig. S2). The additional halogenation thus appears to be an efficient way to increase the chiral ribbons´ widths (with its associated impact on their electronic properties[23]) with only mild annealing treatments.

Knowing that 530 K is not sufficient to drive the lateral cyclodehydrogenative fusion, the presence of radicals must be involved. It seems unlikely that GNRs would display radicals at the 10,10´ positions because they would most probably be immediately saturated by the hydrogen released in intramolecular CDH. We can thus conclude that the lateral fusion must occur in the polymeric phase, when the polymers may still be displaying the radicals at the 10,10´ positions and following the alternative coupling direction outlined in Fig. 1. The fact that most ribbons are only one-monomer wide implies that this lateral coupling is not very effective. This may be ascribed to two different factors that may both contribute, presumably playing together. One is the chiral nature of reactants and polymers, which only allows UC between molecules with the same chirality. The deposited reactants being a racemic mixture, there is a 50% chance for two neighboring polymers to display the same chirality and thereby allow for lateral UC. In addition, the steric hindrance between the up-pointing anthryl units of neighboring polymers sharing the same chirality may interfere and further limit their coupling.

Conclusions

In conclusion, we have evaluated the reactivity of multiple C-Br bonds located at different positions within the same aromatic precursor and observed how the relative distance of the halogens with respect to the substrate results in the selective activation at C_2 sites due to the closer proximity to the catalyst. This favored reactivity promotes one of the possible reaction pathways and limits the product formation to chiral GNRs. Particularly interesting is the fact that substrate-favored debromination at C_2 position overrules the well-known preferred reactivity of acenes at the central rings (C_{10} positions in the case of DBBA precursor). Our results underscore the critical influence of the catalytic substrate on surface-assisted Ullmann coupling. We also demonstrate the use of surface adsorption to design new synthetic strategies that redirect the innate reactivity of aromatic molecules. Specifically, surface adsorption can afford new hierarchical synthetic routes even when carbon atoms are functionalized with the same halogen atoms.

Experimental Section

Experimental Methods

Samples were prepared by deposition of 2,2’,10,10’-tetrabromo-9,9’-bianthracene (see supporting information for the synthesis of this molecule) precursor from Knudsen cell evaporators heated up to 475 K for sublimation. A single crystal Au(111) surface was used as substrate, prepared by standard sputtering/annealing cycles. STM samples analysis was performed at 4.3 K under ultrahigh vacuum (UHV) at pressures below 10^{-10} mbar. All STM images were processed by WSxM software[24].

XPS experiments were performed at the PEARL beamline at the Swiss Light Source (SLS). Samples were prepared using similar conditions to those used for STM experiments. Sample temperatures were calibrated using the readout of two optical pyrometers as a function of sample heating current. The Br 3d signal was monitored during a temperature ramp from RT to 380 °C over the ourse of 8 hours, with each full scan taking approximately 5 minutes (99 scans total). The temperature ramp was performed by incrementally increasing the sample filament current (in direct proximity to the sample) before every scan. A photon energy of 420 eV and an analyser pass energy of 50 eV were used.

Computational Methods

All gas phase calculations were performed using the program ORCA (version 4.0.1.2)[25]. In all calculations we included van der Waals corrections according to the Grimme's D3 approach[26] with the Becke-Johnson damping scheme (D3BJ). We used a triple-zeta quality basis set (def2-TZVP)[25] and the "TightSCF" keyword for all geometry relaxations.

We performed relaxed surface scans to map out the energy profile for the rotation around the single C-C bond connecting the anthracene subunits in TBBA. We also estimated the gas-phase dissociation bond energy for the homolytic cleavage of the C_2-Br and C_{10}-Br bonds in TBBA and in 2,10-dibromoanthracene monomer. The dissociated radical species were calculated at the unrestricted level. Since were are comparing the relative strength between very similar C-Br bonds, zero point energy (ZPE) contributions were not calculated.

For gas-phase calculations, we compared different exchange-correlation functionals, including GGA (PBE)[28] and hybrid, namely, PBE0 and B3LYP [29]. We found that PBE provides a good compromise between accuracy and computational cost for this system and it will be the functional adopted in slab calculations. Finally, since PBE compares well with hybrid functional B3LYP in the energy profile, PBE0 energies were obtained from single point calculations on the PBE-relaxed geometries.

All slab calculations used the PBE exchange-correlation functional[30]. Since we are dealing with physisorbed molecules, we included van der Waals (vdW) corrections via the Grimme's D3 method[26]. We investigated different adsorption sites of the TBBA molecule (chemical formula $C_{28}H_{14}Br_4$) on the Au(111) surface.

The Au(111) surface was modeled with the coordinates derived from the experimental lattice constant of a = 4.0782 Å. The low adsorbate coverage limit was investigated using 8x8x4 slabs (256 Au atoms, 64 atoms per layer) that feature lateral adsorbate separations of ~23 Å between the centers of masses. The computational unit cell was [[L, 0.0, 0.0], [L cos(π/3), L sin(π/3), 0.0], [0.0, 0.0, 32.06365]] Å, where $L=4a\sqrt{2}$. Only the upper two Au layers are allowed to move during geometry relaxations. An ~18 Å vacuum layer and dipole corrections were used to decouple the periodic images along the normal z direction.

For slab calculations, we used the Quickstep (QS)[31] module of the CP2K code [version 6.1, revision number: 18464[30]]. QS solves the electronic problem using a hybrid basis set approach that combines Gaussian and plane wave basis sets. The valence Kohn-Sham orbitals were expanded in a double-zeta quality basis set (DZVP-MOLOPT-GTH for the adsorbate, MOLOPT-DZVP-SR-GTH for Au atoms), which is specifically optimized for its use with the GTH pseudopotentials[33]. The valence electronic density was expanded using a fully converged plane wave cutoff of 600 Ry. All CP2K calculations were carried out at the converged 3x3x1 K point sampling and employed an electronic Fermi-Dirac smearing temperature of 300 K. Geometry relaxations were stopped once the maximum ionic force on any atom fell below 1.0e-3 a.u. (0.05 eV/angstrom). Finally, we double-checked our slab CP2K calculations with the code GPAW [34] and found consistent results.

Acknowledgements

The project leading to this publication has received funding from the European Research Council (ERC) under the European Union's Horizon 2020 research and innovation programme (grant agreement No 635919), from the Spanish Ministry of Economy, Industry and Competitiveness (MINECO, Grant Nos. MAT2016-78293-C6-R), We also acknowledge financial support from the Xunta de Galicia (Centro singular de investigación de Galicia, accreditation 2016–2019, ED431G/09) and Fondo Europeo de Desarrollo Regional (FEDER). This work used the "Imbabura" computer cluster of Yachay Tech University, which was purchased under contract No. 2017-024 (SIE-UITEY-007-2017). A.P.P. thanks D.J. Mowbray for his assistance with the computer cluster. We acknowledge the Paul Scherrer Institut, Villigen, Switzerland for provision of synchrotron radiation beamtime at PEARL beamline and would like to thank N. P. M. Bachellier and M. Muntwiller for assistance. We thank R. Fasel and R. Widmer for provision of substrate and sample holder for the synchrotron experiments.

Keywords: Density functional calculations • Graphene nanoribbons • Hierarchical synthesis • Scanning probe microscopy • Ullmann coupling

[1] S. E. Thompson y S. Parthasarathy, *Mater. Today* **2006**, 9, 20-25.

[2] a) A. Gourdon in *On-Surface Synthesis*, Springer International Publishing, Switzerland, **2016**. b) D. G. de Oteyza, C. Rogero in *On-Surface Synthesis II*, Springer International Publishing AG, **2018**. c) S. Clair y D. G. de Oteyza, *Chem. Rev.* **2018**.

[3] T. Ogawa in *Molecular Electronics*, Springer International Publishing AG, New York, **2017**.

[4] a) A. Gourdon, *Angew. Chem. Int. Ed.* **2008**, 47, 6950-6953.b) G. Franc y A. Gourdon, *Phys. Chem. Chem. Phys.* **2011**, 13, 14283.

[5] V. K. Kanuru, G. Kyriakou, S. K. Beaumont, A. C. Papageorgiou, D. J. Watson, y R. M. Lambert, *J. Am. Chem. Soc.* **2010**, 132, 8081-8086.

[6] S. Weigelt, C. Busse, C. Bombis, M. M. Knudsen, K. V. Gothelf, T. Strunskus, C. Wöll, M. Dahlbom, H. Bjørk, E. Lægsgaard, F. Besenbacher, T. R. Linderoth, *Angew. Chem. Int. Ed.* **2007**, 46, 9227-9230.

[7] a) H.-Y. Gao, H. Wagner, D. Zhong, J.-H. Franke, A. Studer, H. Fuchs, *Angew. Chem. Int. Ed.* **2013**, 52, 4024-4028. b) H.-Y. Gao, J.-H. Franke, H. Wagner, D. Zhong, P.-A. Held, A. Studer, H. Fuchs, *J. Phys. Chem. C.* **2013**, 117, 18595-18602. c) Y.-Q. Zhang, N. Kepčija, M. Kleinschrodt, K. Diller, S. Fischer, A. Papageorgiou, F. Allegretti, J. Björk, S. Klyatskaya, F. Klappenberger, M. Ruben, J. V. Barth, *Nat. Commun.* **2012**.

[8] a) D. Zhong, J.-H. Franke, S. K. Podiyanachari, T. Blomker, H. Zhang, G. Kehr, G. Erker, H. Fuchs, l. Chi, *Science* **2011**, 213-216. b) G. Otero, G. Biddau, C. Sánchez-Sánchez, R. Caillard, M. F. López, C. Rogero, F. J. Palomares, N. Cabello, M. A. Basanta, J. Ortega, J. Méndez, A. M. Echavarren, R. Pérez, B. Gómez-Lor, J. A. Martín-Gago, *Nature* **2008**, 454, 865-868. c) F. Bebensee, C. Bombis, S.-R. Vadapoo, J. R. Cramer, F. Besenbacher, K. V. Gothelf, T. R. Linderoth, *J. Am. Chem. Soc.* **2013**, 135, 2136-2139. d) N. A. A. Zwaneveld, R. Pawlak, M. Abel, D. Catalin, D. Gigmes, D. Bertin, L. Porte, *J. Am. Chem. Soc.* **2008**, 130, 6678-6679. e) M. Abel, S. Clair, O. Ourdjini, M. Mossoyan, L. Porte, *J. Am. Chem. Soc.* **2011**, 133, 1203-1205. f) M. Treier, N. V. Richardson, R. Fasel, *J. Am. Chem. Soc.* **2008**, 130, 14054-14055. g) D. G. de Oteyza, P. Gorman, Y.-C. Chen, S. Wickenburg, A. iss, D. J. Mowbray, G. Etkin, Z. Pedramrazi, H.-Z. Tasi, A. Rubio, M. F. Crommie, *Science* **2013**, 340, 1431-1434. h) M. Di Giovannantonio, G. Contini, *J. Phys. Condens. Matter* **2018**, 30, 093001.

[9] a) F. Ullman, J. Bielecki, *J. Ber. Dtsch. Chem.* **1901**, 34, 2174. b) M. Xi y B. E. Bent, *Surf. Sci.* **1992**, 278, 19-32. c) M. Xi y B. E. Bent, *J. Am. Chem. Soc.* **1993**, 115, 7426-7433. d) S.-W. Hla, L. Bartels, G. Meyer, K.-H. Rieder, *Phys. Rev. Lett.* **2000**, 85, 2777.

[10] L. Grill, M. Dyer, L. Lafferentz, M. Persson, M. V. Peters, S. Hecht, *Nat. Nanotechnol.* **2007**, 2, 687-691.

[11] a) M. Di Giovannantonio, M. Tomellini, J. Lipton-Duffin, G. Galeotti, M. Ebrahimi, A. Cossaro, A. Verdini, N. Kharche, V. Meunier, G. Vasseur, Y. Fagot-Revurat, D. F. Parepichka, F. Rosei, G. Contini, *J. Am. Chem. Soc.* **2016**, 138, 16696-16702. b) M. Abadía, M. Ilyn, I. Piquero-Zulaica, P. Gargiani, C. Rogero, J. E. Ortega, J. Brede, *ACS Nano* **2017**, 11,

12392-12401. c) C. Bombis, F. Ample, L. Lafferentz, H. Yu, S. Hecht, C. Joachim, L. Grill, *Angew. Chem. Int. Ed.* **2009**, 48, 9966-9970. d) G. Vasseur, Y. Fagot-Revurat, M. Sicot, B. Kierren, L. Moreau, D. Malterre, zL. Cardenas, G. Galeotti, J. Lipton-Duffin, F. Rosei, M. Di Giovannantionio, G. Contini, P. Le Fèvre, F. Bertran, L. Liang, V. Meunier, D. F. Perepichka *Nat. Commun.* **2016**, 7, 10235. e) M. Lackinger, *Chem. Commun.* **2017**, 53, 7872-7885. f) M. Kolmer, R. Zuzak, A. K. Steiner, L. Zajac, M. Engelund, S. Godlewski, M. Szymonski, K. Amsharov, *Science* **2019**, 363, 57-60. g) M. Bieri, M.-T. Nguyen, O. Gröning, J. Cai, M. Treier, K. Aït-Mansour, P. Ruffieux, C. A. Pignedoli, D. Passerone, M. Kastler, K. Müllen, R. Fasel, *J. Am. Chem. Soc.* **2010**, 132, 16669-16676. h) R. Gutzler, H. Walch, G. Eder, S. Kloft, W. M. Heckl, y M. Lackinger, *Chem. Commun.* **2009**, 29, 4456.

[12] C. Pigot, F. Dumur, *Materials* **2019**, 12, 662.

[13] a) J. Eichhorn, D. Nieckarz, O. Ochs, D. Samanta, M. Schmittel, P. J. Szabelski, M. Lackinger, *ACS Nano* **2014**, 8, 7880-7889. b) C. Bronner, T. Marangoni, D. J. Rizzo, R. A. Durr, J. H. Jørgensen, F. R. Fischer, M. F. Crommie, *J. Phys. Chem. C* **2017**, 121, 18490-18495. c) M. Di Giovannantonio, J. I. Urgel, R. Widmer, T. Dienel, S. Stolz, C. Sánchez-Sánchez, M. Muntwiler, T. Dumslaff, R. Berger, A. Narita, X. Feng, K. Müllen, P. Ruffieux, R. Fasel, *ACS Nano* **2017**, 12, 74-81. d) C. Bronner, R. A. Durr, D. J. RIzzo, Y.-L. Lee, T. Marangoni, A. M. Kalayjian, H. Rodriguez, W. Zhao, S. G. Louie, F. R. Fishcer, M. F. Crommie, *ACS Nano* **2018**, 12, 2193-2200. e) L. Lafferentz, V. Eberhardt, C. Dri, C. Africh, G. Comelli, F. Esch, S. Hecht, L. Grill, *Nat. Chem.* **2012**, 4, 215-220. f) G. Galeotti, M. Di Giovannantonio, J. Lipton-Duffin, M. Ebrahimi, S. Tebi, A. Verdini, L. Floreano, Y. Fagot-Revurat, D. F. Perepichka, F. Rosei, G. Contini, *Faraday Discuss.* **2017**, 204, 453-469. h) M. Kittelmann, M. Nimmrich, R. Lindner, A. Gourdon, A. Kühnle, *ACS Nano* **2013**, 7, 5614-5620. i) S. Kawai, S. Nakatsuka, T. Hatakeyama, R. Pawlak, T. Meier, J. Travey, E. Meyer, A. S. Foster, *Sci. Adv.* **2018**, 4.

[14] a) D. G. de Oteyza, A. García-Lekue, M. Vilas-Varela, N. Merino-Díez, E. Carbonell-Sanromà, M. Corso, G. Vasseur, C. Rogero, E. Guitián, J. I. Pascual, J. E. Ortega, Y. Wakayama, D. Peña, *ACS Nano* **2016**, 10, 9000-9008. b) J. Cai, P. Ruffieux, R. Jaafar, M. Bieri, T. Braun, S. Blankenburg, M. Muoth, A. P. Seitsonen, M. Saleh, X. Feng, K. Müllen, R. Fasel, *Nature* **2010**, 466, 470. c) P. Han, K. Akagi, F. F. Canova, H. Mutoh, S. Shiraki, K. Iwaya, P. S. Weiss, N. Asao, T. Hitosugi, *ACS Nano* **2014**, 8, 9181-9187.

[15] a) C. Sánchez-Sánchez, T. Dienel, O. Deniz, P. Ruffieux, R. Berger, X. Feng, K. Müllen, R. Fasel, *ACS Nano* **2016**, 10, 8006-8011. b) F. Schulz, P. H. Jacobse, F. F. Canova, J. van der Lit, D. Z. Gao, A. van der Hoogenband, P. Han, R. J. M. Klein Gebbink, M.-E. Moret, P. M. Joensuu, I. Swart, P. Liljeroth *J. Phys. Chem. C* **2017**, 121, 2896-2904.

[16] a) V. V. Cherkez, V. V. Zheltov, C. Didiot, B. Kierren, Y. Fagot-Revurat, D. Malterre, B. V. Andryushechkin, G. M. Zhidomirov, K. N. Eltsov, *Phys. Rev. B* **2016**, 93, 045432. b) V. V. Zheltov, V. V. Cherkez, B. V. Andryushechkin, G. M. Zhidomirov, B. Kierren, Y. Fagot-Revurat, D. Malterre, K. N. Eltsov, *Phys. Rev. B* **2015**, 89, 195425.

[17] M. di Giovannantonio, O. Deniz, Jose I. Urgel, R. Wilmer, T. *Dienel, S.* Stolz, C. Sánchez-Sánchez, M. Muntwiler, T. Dumslaff, R. berger, A. Narita, X. Feng, K. Müllen, P. Ruffieux, R. Fasel, *ACS Nano,* **2017**, 12, 74-81.

[18] C. Bronner, J. Björk, P. Tegeder, *J. Phys. Chem. C* **2015**, 119, 486-493.

[19] a) K. Fukui, T. Yonezawa, H. Shingu, *J. Chem. Phys.* **1952**, 20, 5.b) K. Fukui, T. Yonezawa, C. Nagata, H. Shingu, *J. Chem. Phys.* **1954**, 11, 1453. c) S. S. Zade, N. Zamoshchik, A. R. Reddy, G. Fridman-Marueli, D. Sheberla, M. Bendikov, *J. Am. Chem. Soc.* **2011**, 133, 10803-10816. d) S. S. Zade, M. Bendikov, *J. Phys. Org. Chem.* **2012**, 25, 452-461.

[20] J. Björk, F. Hanke, S. Stafström, *J. Am. Chem. Soc.* **2013**, 135, 5768-5775.

[21] a) A. Mairena, M. Baljozovic, M. Kawecki, K. Grenader, M. Wienke, K. Martin, L. Bernard, N. Avarvi, A. Terfort, K. H. Ernst, C. Wäckerlin, *Chemical Science* **2019**, 10, 2998-3004. b) C. Bronner, J. Björk, P. Tegeder, *J. Phys. Chem .C.,* **2015**, 1, 486-493.

[22] a) H. Huang, D. Wei, J. Sun, S. L. Wong, Y. P. Feng, A. H. C. Neto, A. T. S. Wee, *Sci. Rep.* **2012**, 983. b) S. Wang, N. Kharche, E. Costa Girão, X. Feng, K. Müllen, V. Meunier, R. Fasel, P. Ruffieux, *Nano Lett.* **2017**, 17, 4277-4283. c) Z. Chen, H. I. Wang, N. Bilbao, J. Teyssandier, T. Prechtl, N. Cavani, A. Tries, R. Biagi, V. De Renzi, X. Feng, M. Kläui, S. de Feyter, M. Bonn, A. Narita, K. Müllen, *J. Am. Chem. Soc.* **2017**, 139, 9483-9486. d) C. Ma, L. Liang, Z. Xiao, A. A. Puretzky, K. Hong, W. Lu, V. Meunier, J. Bernholc, A.-P. Li, *Nano Lett.* **2017**, 17, 6241-6247. e) O. Deniz, C. Sánchez-Sánchez, T Dumslaff, X. Feng, A. Narita, K. Müllen, N. Kharche, V. Meunier, R. Fasel, P. Ruffieux, *Nano Lett.* **2017**, 17, 2197-2203. f) A. Basagni, F. Sedona, C. A. Pignedoli, M. Cattelan, L. Nicolas, M. Casarin, M. Sambi. *J. Am. Chem. Soc.* **2015**, 137, 1802-1808. g) N. Merino-Díez, A. Garcia-Lekue, E. Carbonell-Sanromà, J. Li, M. Corso, L. Colazzo, F. Sedona, D. Sánchez-Portal, J. I. Pascual, *ACS Nano* **2017**, 11, 11661-11668. h) N. Merino-Díez, J. Lobo-Checa, P. Nita, A. Garcia-Lekue, A. Basagni, G. Vasseur, F. Tiso, F. Sedona, P. K. Das, J. Fujii, I. Vobornik, M. Sambi, J. I. Pascual, J. E. Ortega, D. G. de Oteyza, *J. Phys. Chem. Lett.* **2018**, 9, 2510-2517.

[23] Martina Corso, Eduard Carbonell-Sanromà, Dimas G. de Oteyza in *Bottom-Up Fabrication of Atomically Precise Graphene Nanorribons*, Springer-Cham, **2017**.

[24] I. Horcas, R. Fernández, J. M. Gómez-Rodríguez, J. Colchero, J. Gómez-Herrero, A. M. Baro, *Rev. Sci. Instrum.* **2007**, 78, 013705.

[25] F. Neese, *Wiley Interdiscip. Rev. Comput. Mol. Sci.* **2012**, 2, 73-78.

[26] a) S. Grimme, S. Ehrlich, L. Goerigk, *J. Comput. Chem.* **2011**, 32, 1456-1465. b) S. Grimme, J. Antony, S. Ehrlich, H. Krieg, *J. Chem. Phys.* **2010**, 132, 154104.

[27] F. Weigend, R. Ahlrichs, *Phys. Chem. Chem. Phys.* **2005**, 7, 3297.

[28] C. Adamo, V. Barone, *J. Chem. Phys.* **1999**, 110, 6158-6170.

[29] a) A. D. Becke, *J. Chem. Phys.* **1993**, 98, 5648-5652. b) P. J. Stephens, F. J. Devlin, C. F. Chabalowski, M. J. Frisch, *J. Phys. Chem.* **1994**, 98, 11623-11627.

[30] J. P. Perdew, K. Burke, M. Ernzerhof, *Phys. Rev. Lett.* **1996**, 77, 3865-3868.

[31] J. VandeVondele, M. Krack, F. Mohamed, M. Parrinello, T. Chassaing, J. Hutter, *Comput. Phys. Commun.* **2005**, 167, 103-128.

[32] J. Hutter, M. Iannuzzi, F. Schiffmann, J. VandeVondele, *Wiley Interdiscip. Rev. Comput. Mol. Sci.* **2014**, 4, 15-25.

[33] S. Goedecker, M. Teter, J. Hutter, *Phys. Rev. B* **1996**, 54, 1703-1710.

[34] a) J. J. Mortensen, L. B. Hansen, K. W. Jacobsen, *Phys. Rev. B* **2005**, 71, 2005. b) J. Enkovaara, C. Rostgaard, J. J. Mortensen, J. Chen, M. Dulak, L. Ferrighi, J. Gavnholt, C. Glinsvad, V. Haikola, H. A. Hansen, H. H. Kristoffersen, M. Kuisma, A. H. Larsen, L. Lehtovaara, M. Ljungberg, O. Lopez-Acevedo, P. G. Moses, J. Ojanen, T. Olsen, V. Petzold, N. A. Romero, J. Stausholm- Møller, M. Strange, G. A. Tritsaris, M. Vanin, M. Walter, B. Hammer, H. Häkkinen, G. K. Madsen,

R. M. Nieminen, J. K. Nørskov, M. Puska, t. T. Rantala, J. Schiøtz, K. S. Thygesen, K. W. Jacobsen, *J. Phys. Condens. Matter* **2010**, 22, 253202.

ARTICLE

Possible synthetic routes expected in this experiment. The presence of carbon-bromine bonds with similar gas-phase binding energies in principle allows the Ullmann coupling to occur via two different orientations. However, upon adsorption on Au(111), only one type of carbon-bromine bond is preferentially cleaved, thus selecting coupling route (#2, in the figure) to the formation of chiral graphene nanoribbons. Ocasionally, some non-favored carbon-bromine bonds are also cleaved leading to the lateral fussion of the nanoribbons.

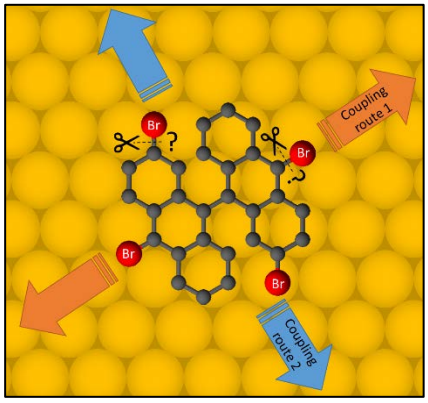

*Néstor Merino-Díez, Alejandro Pérez Paz, Jingcheng Li, Manuel Vilas-Varela, James Lawrence, Mohammed S. G. Mohammed, Alejandro Berdonces-Layunta, Ana Barragán, J. Ignacio Pascual, Diego Peña and Dimas G. de Oteyza**

1 - 5

Hierarchy in the halogen activation during surface-promoted Ullmann coupling